Journal Name

ARTICLE TYPE

Cite this: DOI: 00.0000/xxxxxxxxxx

Aggregation Structure of Chiral Cubic Liquid Crystals Revealed by X-ray Diffraction Utilizing a New Algorithm†

Toshihiko Oka,[a] Yasuhisa Yamamura,[b] Shoichi Kutsumizu,[c] and Kazuya Saito*[b]

Received Date
Accepted Date

DOI: 00.0000/xxxxxxxxxx

Chiral aggregation structure spontaneously formed by achiral rodlike molecules, a long-time unsolved problem in liquid crystal science, has been clarified by applying a new crystallographic algorithm recently developed while utilizing aggregation characteristics of this type. Bicontinuously interwoven networks characterize it similarly to the neighboring Gyroid phase in a phase diagram against the alkyl chain length and temperature. However, the network connectivity is significantly different from the bicontinuous networks that have been either known for related compounds or assumed for this phase. The network is compatible with the homochiral arrangement of rodlike molecules with successive twists by a proper angle between adjacent junctions.

1 Introduction

The chirality of molecular systems has been a significant subject in natural science.[1–4] Among related issues, its emergence in self-assembled systems from achiral ones is a great question and believed as a critical event in the origin of life.[5–7] Although some examples, including spontaneous resolution into chiral crystals,[8] have been identified in nature,[9,10] we still need other examples to understand the underlying mechanism(s) of its emergence. The formation of the chiral phase composed of achiral molecules offers handy and tractable systems suitable for detailed study. In this regard, producing and identifying such achiral molecules are challenges in soft matter science. The subject of this paper is a chiral cubic phase in thermotropic liquid crystals formed by achiral molecules.[11]

Thermotropic cubic phases are mesophases appearing between a well-ordered crystal and the isotropic liquid upon temperature variation.[12] They have a large cubic unit cell containing ca. 10^3 molecules and often appear at higher temperatures than ordinary liquid crystalline phases, such as smectic phases. Thus, molecules travel by diffusional process and reorientations, resulting in severe disorder at the atomic scale. Despite the difficulties, the averaged molecular packing in some of cubic phases has been well established.[13–15] In the long history of the study of thermotropic cubic liquid crystals, 1,2-bis(4'-*n*-alkyloxybenzoyl)hydrazine [abbreviated as BABH(*n*), shown in Fig. 1] and 4'-*n*-alkoxy-3'-nitrobiphenyl-4-carboxylic acid [ANBC(*n*)] are the most famous and representative.[12,16–22] Remarkably, they both exhibit two types of cubic phases depending on the length of the alkyl chain, *n*. The two phases at short- and long-chain regime share the fundamental structure, by which we call them the Gyroid phases. The structure analysis for BABH(*n*) was the first to present a twisted arrangement of molecules in the Gyroid phases.[13] A phase sandwiched by the two Gyroid phases has been revealed to be chiral despite achiral constituent molecules.[11] Three groups,[11,23–26] including us, proposed models of its molecular aggregation, but these are more or less hand-carved based on assumptions, which might be justified at their moments but without firm logic, such as supposed resemblance to the "ideal" centrosymmetric structure. Solving this puzzle by revealing the aggregation structure of the chiral phase should contribute to deepening our understanding of the emergence of chirality in ensembles of achiral molecules. It is also technologically significant for designing such chiral assemblies of new functionalities.[10,27,28]

The most significant problem in revealing molecular aggregation is the so-called phase problem in diffraction crystallography for systems without inversion symmetry. The lack of centrosymmetry significantly widens the search space from discrete (combinations of either sign for structure factors corresponding to 0 and

[a] *Department of Physics, Faculty of Science, and Nanomaterials Research Division, Research Institute of Electronics, Shizuoka University, Shizuoka 422-8529, JAPAN.*
[b] *Department of Chemistry, Faculty of Pure and Applied Sciences, University of Tsukuba, Tsukuba, Ibaraki 305-8571, JAPAN. E-mail: kazuya@chem.tsukuba.ac.jp*
[c] *Department of Chemistry and Biomolecular Science, Faculty of Engineering, Gifu University, Yanagido, Gifu 501-1193, JAPAN.*

† The following files are available free of charge. SupportingInformation.pdf: Definitions of the indicators minimized, the adopted generalization of the algorithm for powder diffraction data, summarizing graphs of analyses starting from 100 random guesses and graphs showing the resultant distribution of the phases of structure factors reached in the best results, the retrieved structure factors, the electron density distribution of BABH(15), some geometric quantities with information of phase sequence, representation of aggregation structures of the chiral and achiral Gyroid phases in terms of triangles, and the detailed discussion reaching to the packing model in Fig. 5. BABH14_electrondensity.mp4: Movie representing the electron density in a unit cell of BABH(14). skeletons.mp4: Movie representing the skeletal graphs rotating around a body diagonal of a unit cell of the chiral cubic phase. cylinders.mp4: Movie representing the aggregation model in Fig. 4 rotating around a body diagonal of a unit cell of the chiral cubic phase.

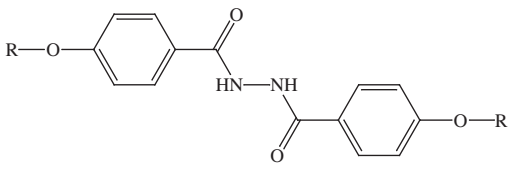

Fig. 1 Molecular Structure of BABH(n) (R = C_nH_{2n+1}).

π as phases) to continuous ones (possible phases being real numbers between $-\pi$ and π). Recently, one of the present authors has shown the successful and computer-aided deduction of the combination of phases based on physical (structural) features in highly disordered and nano-segregated systems.[29,30] The fundamental observations are that the continuous electron density compatible with molecular diffusion accompanies the small density modulation and integral of absolute "curvature" in the four-dimension. The latter is a mathematical expression for what isolated maximum and minimum of the electron density are implausible. The minimization of two indicators reflecting these observations gave correct structures for test data. This communication utilizes the strategy to reveal the molecular aggregation in the chiral cubic phase of BABH(n). Previous studies[12,31,32] have indicated that they are suitable targets for the algorithm. In the molecule, the hydrazine moiety (-HN-NH-) at the center has the highest electron density.[13]

2 Analysis

We performed iterative analyses using a homemade program[30] while incorporating optimization for overlapped diffractions in powder diffraction (see Supporting Information[†] for the algorithm generalization and raw diffraction patterns). The input data are the same as those used in previous MEM analyses[33] (assuming the inversion symmetry as was common at the time). Initial combinations of phases in $(-\pi,\pi]$ were randomly generated while adopting the Friedel law. The unit cell is voxelized as $32\times32\times32$ while considering the largest norm of the diffraction wavevector utilized. We set the analysis condition so that the larger density parts form networks, considering the aggregation structure of the Gyroid phase of BABH(n) with different chain lengths n.[13,15] The number of the initial combinations is 100 for each compound. Since the algorithm does not guarantee the convergence to the true solution, we compare the converged results in two indicators, I_ρ and I_K, introduced in the previous papers[29,30] (see Supporting Information[†] for their definitions). Note that the previous paper[29] indicates that I_K is more important for choosing a better solution. In the case of BABH(14), 71 of 100 analyses converged on mostly identical electron density distributions, and 20 of them consistently yielded solutions with numerically identical indicators of the smallest I_K. For BABH(15), essentially identical distributions were in 79 analyses, and the number of the smallest I_K solutions was 14. Remarkably, the best solutions for the two compounds give indistinguishable electron densities after appropriate operations such as reflection, rotation, translation, and their combination. Note that the algorithm does not require any candidates of space groups for the structure beyond the fundamental level, such as cubic symmetry. We assign it to the structure based on the resultant electron density distribution. The assignment is used to calculate the averaged phases and their standard deviations for structure factors interrelated under the assigned space group.

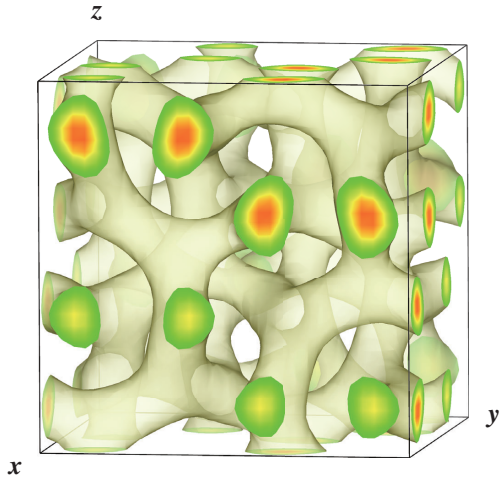

Fig. 2 Electron density [orange (high) → yellow → green (low)] in a unit cell of the chiral cubic phase of BABH(14). A region with a positive electron density than a threshold is shown. The electron density has been translated to match the conventional origin of $I2_13$. A movie showing sections of the electron density is available as a supplementary file.[†]

3 Results and discussion

3.1 Electron density and space group

Figure 2 illustrates the resulting electron density distribution in a unit cell for the best solution of BABH(14) (that for BABH(15) in Supporting Information[†]). These distributions resemble that with the $Ia\bar{3}$ symmetry but have the $I2_13$ symmetry, as explained in the next paragraph. We find a regular network structure, as expected. In reality, the structure consists of two interwoven networks. Note that the electron density distribution in Fig. 2 is not an artificially constructed (hand-carved) model but a direct result of the analysis by the algorithm, behind which a plausible assumption catching the aggregation features exists. Since it comes as a simple Fourier synthesis, it precisely gives the input intensities if Fourier-transformed.

Analyses of retrieved phases for reflections and relations among them,[34] along with the extinction rule, pointed to the chiral space group $I2_13$ as the most plausible. The followings are essential: the optimized phases of some reflections close to integer multiples of $\pi/2$ and relations such as signs among them. The numerical results of the best solutions are shown in Table 1. Phases for equivalent diffractions converged to the equivalent value within reasonably small uncertainties except for {422} of BABH(14), small $|F|$ of which affects little the resulting electron density distribution. It is an indication of reasonable convergence. Remarkably, some indices converged to phases significantly different from fractional multiples of π. We had no possibility of reaching these results without any optimization scheme. The algorithm proposed in the

Table 1 Structure factors (amplitude $|F(hkl)|^{\ddagger}$ and phase ϕ with standard deviation σ_ϕ) of the chiral cubic phase of BABH(14) and BABH(15) assuming the space group $I2_13$.

					BABH(14)			BABH(15)		
h	k	l	multiplicity	$\phi_{ex}{}^{\P}/\pi$	$\|F(hkl)\|$	$\phi(hkl)/\pi$	σ_ϕ/π	$\|F(hkl)\|$	$\phi(hkl)/\pi$	σ_ϕ/π
3	1	0	12	$-\frac{1}{2}$ or $\frac{1}{2}$	0.0550	0.514	0.023	0.0375	0.504	0.019
1	3	0	12	$-\frac{1}{2}$ or $\frac{1}{2}$	0.2434	-0.505	0.010	0.2383	-0.499	0.003
2	2	2	8		0.4098	0.379	0.012	0.4016	0.416	0.002
3	2	1	24		0.7217	0.030	0.011	0.6873	0.0614	0.0011
2	3	1	24		0.7966	0.019	0.004	0.7552	0.0165	0.0008
4	0	0	6	0 or 1	1.0000	-0.9998	0.0002	1.0000	-0.9999	0.0002
4	1	1	24		0.2252	0.817	0.014	0.1973	0.812	0.006
3	3	0	12	$-\frac{1}{2}$ or $\frac{1}{2}$	0.0337	0.490	0.016	0.0389	0.495	0.013
4	2	0	12	0 or 1	0.2425	0.010	0.028	0.2372	-0.0001	0.0011
2	4	0	12	0 or 1	0.2788	-0.999	0.011	0.2513	1.000	0.002
3	3	2	24		–	–	–	0.0663	-0.063	0.007
4	2	2	24		0.1207	-0.866	0.188	0.0908	-0.595	0.017
4	3	1	24		0.0769	-0.093	0.046	0.0775	-0.114	0.005
3	4	1	24		0.0454	0.947	0.057	0.0444	0.956	0.012
5	1	0	12	$-\frac{1}{2}$ or $\frac{1}{2}$	0.0378	-0.502	0.003	0.0460	-0.499	0.002
1	5	0	12	$-\frac{1}{2}$ or $\frac{1}{2}$	0.0077	-0.471	0.046	0.0029	0.478	0.034
5	2	1	24		–	–	–	0.0547	0.871	0.010
2	5	1	24		–	–	–	0.0286	-0.250	0.017

‡ $|F(hkl)| \neq |F(khl)|$ in general for the Laue class $m\bar{3}$ covering $I2_13$, whereas the cyclic permutations of hkl retain the amplitude.
¶ Expected phases under $I2_13$.[34] Blank indicates the absence of restrictions by the symmetry.

previous papers[29,30] has opened a way to consider the possibility. Note that the algorithm does not discriminate absolute structures, i.e., mirror images. The analyses yield them by equal probabilities when started from random phases. The indistinguishability necessitates the reflection for a meaningful comparison of analysis results.

3.2 Network geometry: Interwoven *noh* nets

Figure 3a shows skeletal graphs of the electron density. The vertices are located on the local maxima of the electron density. Crystallographically, it suffices to put two on a threefold axis (which contains a body diagonal) and two at general positions (see Supporting Information† for their fractional coordinates). An achiral space group $Ia\bar{3}$ suffices to represent the graphs with two independent vertices on a threefold axis and a general position. Two interpenetrating (interwoven) line graphs (yellow and bluish), which contain six-membered and ten-membered circuits, are related by a half translation along a body diagonal. Each network is topologically a *noh* net,[35] of which the idealized space-group symmetry is $Pa\bar{3}$ with an equal distance of $0.217a$ (in terms of the lattice constant, a) among the connected junctions that are entirely flat. The comparison is in Fig. 3b for the bluish and ideal nets (see Supporting Information† for separate drawings). The deviations of the obtained vertices from the ideal ones are $0.05a$ at most. The interlocking of the two distorted *noh* graphs happens only between the ten-membered circuits of the respective graphs (see a supplementary movie). An example of the six-membered circuit is colored pale blue in Fig. 3a. The six-membered circuit deformed into the so-called chair-form (of cyclohexane molecules) is at a body center and sandwiched by two three-way junctions (orange), whose outgoing connections are rotated by $\pi/3$ around the common threefold axis (a body diagonal of the cell). The stacking of motifs along the axis is represented as $\ldots 3_B 3_Y S_B 3_Y{}' 3_B{}' S_Y \ldots$ (no S_Y in Fig. 3a) using 3 for a three-way junction, S for a six-membered circuit, and Y and B for the color indicator of graphs. The apostrophe distinguishes distinct three-way junctions. Three-way junctions with different orientations connect to each vertex of the six-membered circuit. The stacked structure of two three-way junctions and a hexagonal hole reminds us of the so-called mesh phase in lyotropic systems (hexagonally perforated lamellar phase in polymers).[36]

At this stage, we need to assess whether the result is probable or not. The answer is yes. There exist at least five points to note:

- All junctions are three-way. This property is common to the Gyroid phase and beneficial for molecules to assemble in a twisted manner of a single sense along the network.[24] In the Gyroid phase, the necessary twist angle between junctions is $\arccos\frac{1}{3}$ ($\approx 70.5^\circ$), whereas those for the ideal *noh* net are ca. 65°. Although actual junctions are slightly out of a flat plane, slight adjustment suffices for molecular arrangement.

- The distances between adjacent vertices $0.22a(I2_13)$ (on average) are almost equal to the interjunction distance, $(\sqrt{2}/4)a$(Gyroid), of neighboring Gyroid phases of compounds with different alkyl chains (see Table S2 in Supporting Information†). The twisting necessary for assembling will be mostly uniform.

- The number of junctions per cell is 64, 4 times larger than the Gyroid phase. The number reasonably explains the ratio of $a(I2_13)/a$(Gyroid) for BABH(15) (≈ 1.57) by $4^{1/3} \approx 1.59$, assuming an equal number of molecules per junction.

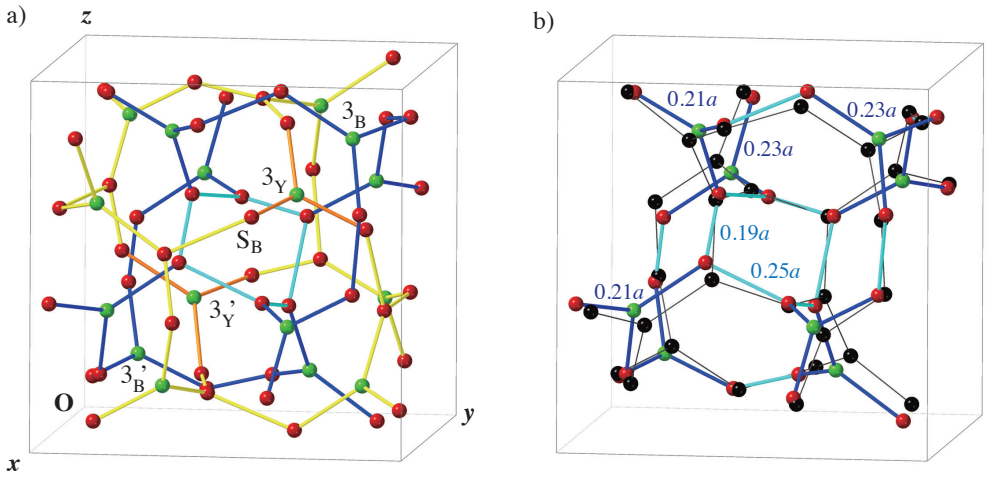

Fig. 3 Skeletal graphs (nets). a) Graphs deduced from the electron density in a unit cell of the chiral cubic phase of BABH(n). Yellow and bluish graphs are bicontinuously interwoven. Sixteen green spheres are on threefold axes (including a body diagonal), whereas 48 red ones are at crystallographically general positions. A movie rotating the networks is available as a supplementary file.† b) Comparison of the bluish net and the ideal *noh* net (black). In the bluish net, light and deep blue distinguish the connections between vertices at general positions and those involving the vertices on a threefold axis. Selected distances in the bluish net are given in a unit of the cell constant, a. All distances are $0.217a$ in the ideal net.

- The subtlety of the formation condition has been known between the *noh* net and the *srs* net, of which a chiral pair represents the skeletal graph of the Gyroid phase.[35] For the so-called metal-organic framework (MOF) coordination polymers, a slight change in the synthesis condition resulted in the formation of either the *srs* or *noh* nets sharing the chemical components.[35,37,38]

- The molecular aggregation derived from the graph reasonably explains the chain-length dependence of the cell constant,[18] as will be described later.

All of the above points do not interfere with but enhance the plausibility of the obtained structure.

3.3 Chiral molecular aggregation

Although the skeletal graphs are compatible with the inversion symmetry of $Ia\bar{3}$, the reality is chiral. The vertices of the six-membered circuit are at general positions under $I2_13$. This fact results in the disproportion of the edge lengths into $0.19a$ and $0.25a$ in alternation (see Fig. 3b). Their distances from vertices on a threefold axis are also different, $0.21a$ and $0.23a$. Thus, the locations of vertices already indicate the chirality. Besides, their spatial arrangement seems to offer a suitable stage of chiral assembly with homochiral twisting. As shown in Fig. 4, we can place rodlike molecules on the graphs. Since all junctions are not strictly planar, distinctly from the Gyroid phase and the ideal *noh* net, we cannot precisely specify, to any connections between the adjacent junctions, the twisting mode, including the twist angle along the connection. However, the sense of twist along the six-membered circuit is unique by its non-planarity if we assume a smaller twist than $\pi/2$ for the shorter edge. This sense is compatible with the natural senses of the connections (with an angle less than $\pi/2$) to the vertices on a threefold axis. Thus, the natural sense of the six-membered circuit consistently extends to a whole graph (say, blueish). Then, the body-centered lattice forces the sense of the other network (yellow) to be the same as the bluish network.

Unless some extrinsic factors prevent it, the homochirality is preferential while ignoring a weak entropy effect, as exemplified by induction of cholesteric, i.e., chiral nematic phases by a tiny amount of chiral dopant to achiral nematic phases.[39] The three-way junctions in Gyroid phases stacked along threefold axes (including body diagonals) are forced to alternate in twist sense by the orientations at the vertices,[13] which locates at the high symmetry points. Since the micro phase-separation pattern of the Gyroid phase is highly stable even without taking the chirality into account,[40–44] the twist sense at junctions seems more fundamental than the interaction between domains with opposing chirality. As described later, the recognition of the fundamental importance of not a segmental but surface aggregation is essential in this reasoning. On the other hand, in the present case, we identify no such restriction. The stack of the two three-way junctions (3_B and 3_Y) at the upper part of Fig. 4 implies that the same sense of twist on the neighboring networks stabilizes the aggregation by minimizing the steric interference of alkyl tails on both molecular ends, besides adjusting the distances between them, as discussed below.

3.4 Alkyl packing

The orientation of the molecules at the junctions on body diagonals is parallel to them on average by symmetry, similar to the Gyroid phase. Based on this parallel arrangement, we revealed the details of molecular aggregation in the Gyroid phase.[15] Considering the possible variety of alkyl-chain orientations and interdigitations,[15,45–47] we can imagine the molecular arrangement reasonably compatible with the reported chain-length dependence of the cell constant[18] (see Supporting Information† for details), as shown in Fig. 5: the parallel alkyl chains with

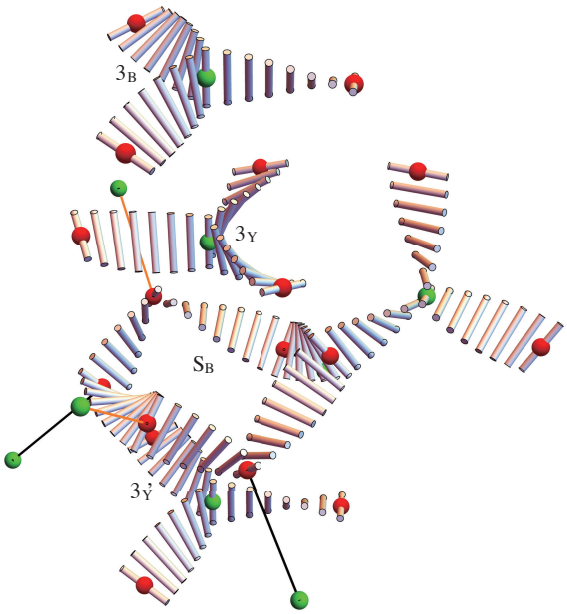

Fig. 4 Averaged and idealized molecular packing ($3_B3_YS_B3_Y'$ from the top to the bottom and a three-way junction associated with the central S_B) along a body-diagonal of a unit cell in the chiral cubic phase of BABH(n). Sphere colors (green and red) distinguish vertices on a threefold axis and at a general position. Outgoing connections from the central six-membered circuit to three-way junctions are, for clarity, indicated by two orange and three black rods for short and long distances, respectively. The circuit edges alternate in length. The length of cylinders roughly corresponds to the core length of BABH(n) molecules. A movie rotating the model is available as a supplementary file.[†]

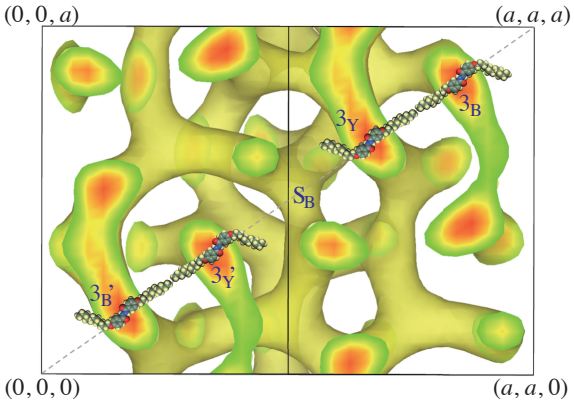

Fig. 5 Packing model of molecules with parallel and bent alkyl chains relative to the molecular core on both ends along a body-diagonal of the unit cell. Since the molecules on the body diagonal are "cylindrical" on average (threefold symmetric according to the system symmetry), the figure indicates only that the bent chains are at the sides of the six-membered circuit, whereas the straight ones between the junctions on the diagonal. The electron density is cut by a plane embedding the diagonal.

little interdigitation between the two junctions on a body diagonal (3_B and 3_Y), and the bent chains directed to the six-membered circuit (S_B). The bent chain conformation at the side of the six-membered circuit is reasonable to fill a space together with chains of molecules on the circuit. This molecular packing explains the chain-length dependence of the cell constant as $(4/\sqrt{3}) \times [(0.19/2)\ \mathrm{nm}\ (\mathrm{CH_2})^{-1} + (0.14/2)\ \mathrm{nm}\ (\mathrm{CH_2})^{-1}] \approx 0.38\ \mathrm{nm}\ (\mathrm{CH_2})^{-1}$.

It is emphasized that the chain disorder in most liquid crystals, including the present cases,[18,31,32] is comparable to that in the isotropic liquid phase and liquid alkanes.[48–50] The molecular conformation perpetually changes from time to time. The orientations of alkyl chains proposed above are literally on average relative to the body diagonal that coincides with the averaged molecular orientation there.[15,45–47] The straight chains do not mean an all-*trans* state at all. Similarly, we do not claim anything concerning the tilt direction (around the body diagonal) of disordered alkyl chains, for which we need further studies having higher sensitivity even for dynamical correlation.

3.5 The $I2_13$ and Gyroid phases

The chiral $I2_13$ phase appears between two regions of the Gyroid/$Ia\bar{3}d$ phases upon the variation of alkyl chain length in BABH(n). The appearance also happens in other series of the representative cubic mesogen, ANBC(n),[19–22] and mixtures of its short-chain member and liquid alkane.[51,52] Thus, the comparison and consideration under this view would contribute to reaching a unified understanding. In the following, we discuss some issues in three aspects.

3.5.1 Three-way junctions

For rodlike molecules to pack reasonably densely, the flat surface is beneficial besides nematic, i.e., the orientationally ordered but positionally disordered state. On the other hand, the segmen-

tal description is beneficial for describing the twisted organization. Then, a question arises which of them is primary? A geometric consideration[13,53] undoubtedly indicated that the surface description is intrinsically superior to the model based on a line graph for systems consisting of rodlike molecules. Chemistry may experimentally check the fundamental importance of the surface description. If the segmental structure is primary, its contribution (linear in the cell constant, a) to the free energy is inferior to that of the interfaces between different chiral domains ($\propto a^2$), resulting in the instability of the Gyroid phase of proportionally large molecules.

The model illustrated in Fig. 4 is only for clarity in describing the twisted arrangements. The junctions correspond to the centers of rounded-triangular planes of molecular aggregations.[13,15] Supporting Information[†] contains idealized representations of the chiral and Gyroid phases in triangles. It is noteworthy that the triangular description of the Gyroid phase exhibits a close similarity to its medial surface.[54]

Since both phases consist solely of three-way junctions, their origin is the next question. They are special doubly as follows: Such junctions can always find a smooth surface that locally embeds a junction and outgoing connections, in contrast to higher branching junctions such as tetrahedral and octahedral ones,[24–26] and the number of branching is minimal among junctions successfully embedded on a local surface. The latter factor may be translated into their easier formation.

3.5.2 Double networks

Construction of the whole assembly by triangular units (three-way junctions) often offers too loose space filling if the construction is singly continuous without self-penetration. Indeed, the present structure (two *noh* nets), as well as the Gyroid phase (two *srs* nets), consists of interwoven nets. Since the formation of a nonequivalent net to fill a void seems physically implausible, we assume the equivalence of two nets hereafter.

All vertices are crystallographically equivalent at special positions without remaining freedom in the Gyroid phase. Each *srs* net is chiral, and they are enantiotropic to each other (related by the inversion). Orientations of connecting triangles are twisted by 70.5° around the segment between the triangle centers (vertices of the net). This twist determines the sense of the twisted orientations of neighboring molecules

On the other hand, the present structure contains two *noh* nets. Since the *noh* net can be achiral, as exemplified by a centrosymmetric space group $Pa\bar{3}$ for the idealized one, the doubled structure in the present case could be achiral with a centrosymmetric $Ia\bar{3}$. An essential difference from the Gyroid phase is the location of two independent vertices: One is restricted on a threefold axis, and the other is at a general position without any restriction. We can regard the centrosymmetric pairs as a state of symmetry. Then, the symmetry guarantees that the free energy of this state is either minimum or maximum. The absence of crystallographic restrictions allows the structure to relax to minimize the free energy. We should regard the found structure described before as a result of this minimization.

The interface of two chiral microdomains of the Gyroid phase is a triply periodic minimal surface (TPMS) known as gyroid in differential geometry.[55] The significance and specialty of the gyroid surface as TPMS offer a possibility to place the Gyroid phase among self-assemblies characterized by TPMSs.[44,54] Indeed, the gyroid surface belongs to a family of TPMSs mutually related by the Bonnet transformation, which keeps the local geometry.[55] Although the local environment of a molecule is the same in phases characterized by the TPMSs, superior stability of the Gyroid phase is rationalized in terms of the surface homogeneity[54] and the Landau theory of weak crystallization.[44]

The interface of two domains assignable to each net of the $I2_13$ phase, evidently a non-TPMS, is to be characterized further in the future. An alternative but somewhat resembling way is to ask why the structure has a superior stability to other structures with similar properties as that characterized by a net. However, the clarification is challenging because the number of mathematically different nets is substantial: Reference[35] lists 16 nets, even for uniform nets involving only three-way junctions like the *srs* net. The task is also left for the future.

3.5.3 Chain-length dependence

The previous studies[13,15] revealed the different molecular packing in two Gyroid phases located at both sides of the chiral $I2_13$ phase on the phase diagram against chain length in multiple compounds, including BABH(n).[18,22] Moreover, other systems also exhibit chiral phases besides the Gyroid phase depending on the alkyl chain length.[56–60] Here, we attempt to place the present findings in this context.

The central portions of molecules form single and double layers in the short- and long-chain regions of the Gyroid phase while retaining the symmetry of the two sides.[13] The change into the double-layered state adjusts the volume fraction of the effective core part. On the other hand, no symptom of an apparent change in the density exists in the aliphatic domains formed by disordred (molten) alkyl chains at both ends of a molecule. Still, the chains change averaged orientation and interdigitation:[15] In the short chain regime, the chains are tilted from the layer normal defined locally, resulting in the molecular bent (on threefold axes), and the interdigitation of the two facing chains extending from core layers is negligible, whereas the chains are normal to the core layers with full interdigitation in the long-chain regime. This change in the alkyl packing happens probably to fit the domain shape.

In the structure revealed in this study, the chain packing is intermediate between the two outside regions (Gyroid phase). According to the two surroundings of alkyl chains, packing modes split into two, resulting in the curved junctions on threefold axes because of the asymmetry of the two sides. The chains in one regions are tilted, whereas those in the other are normal. We assume the latter between the stacked three-way junctions (say, 3_B and 3_Y in Fig. 4), though there is no concrete logic to validate the assumption. However, the asymmetry of the junctions on the threefold axes is consistent with the sign of its curvature (direction of sagging) if we assume that the tilted alkyl conformation tends to fill more space laterally. A bulgy side of the junction seems to fit reasonably a central hole of the six-membered circuit. Note that we cannot assume significant interdigitation for

both sides of the junction on a threefold axis. On the other hand, for the molecular cores, we cannot recognize a symptom of such intermediate aggregation, partly due to the limited spatial resolution of the experimental data. The formation of the six-membered circuit between the three-way junctions plausibly contributes to relaxing structural frustration inconvenient for both states of the Gyroid phase.

Finally, the appearance of the $I2_13$ phase itself offer an important message for the self-assembly of soft matter. Beautiful and complicated structures formed by self-assembly have often been discussed under surface geometry.[55] The concept of minimizing interfacial energy to yield minimal surfaces is fascinating and has largely been successful in polymers and lyotropics. Although the geometric consideration is essential, as discussed in this paper, the appearance of the $I2_13$ presumably indicates the fundamental importance of the resemblance in network geometry (*noh* and *srs* nets) and resulting triangular constructions for systems of molecules having a hard rodlike core and a flexible chain(s).

4 Concluding remarks

The present work has solved a long-standing problem of what aggregation structure is inside a chiral cubic liquid crystal of achiral rodlike mesogens by utilizing a new crystallographic algorithm based on physical insights of molecular dynamics inside. The revealed structure is significantly different from existing models, including ours. Irrespective of explicit statements, the previous models picked some hints from rough estimates of the electron density under the inversion symmetry as a starting point. The present analysis indicates that the assumption is not justified: We needed a physical insight into the formed structure to identify. Two interwoven *noh* nets characterize the structure. The chiral distortion from the idealized achiral net facilitates the homochiral packing of molecules. The characteristics of the aggregation structure enabled the examination of the packing of disordered alkyl groups. Comparison with and consideration of the neighboring Gyroid phases revealed the structural significance of the three-way junctions and double networks in this kind of soft matter. Consequently, this study undoubtedly contributes to revealing the underlying mechanism for the emergence of chirality in the self-assembly of achiral molecules.

Author Contributions

TO, algorithm improvement, phase retrieval, model improvement, and editing the manuscript; YY, model improvements, constructing the chain packing model, and editing the manuscript; SK, model improvements, and editing the manuscript; KS, constructing and improving the aggregation model, first draft preparation, and successive revision.

Conflicts of interest

There are no conflicts to declare.

Acknowledgements

This work was supported in part by JSPS Grant-in-Aid for Scientific Research on Innovative Areas “Discrete Geometric Analysis for Materials Design” (JP20H04634 for TO, JP20H04629 for KS), Grant-in-Aid for Scientific Research (C) (JP20K05619) for SK, and Grant-in-Aid for Scientific Research (B) (JP21H01046) for KS.

Notes and references

1 L.D. Barron, *Chem. Soc. Rev.*, 1986, **15**, 189-223.
2 F. Zaera, *Chem. Soc. Rev.*, 2017, **46**, 7374-7398.
3 E.M.G. Jamieson, F. Modicom and S.M. Goldup, *Chem. Soc. Rev.*, 2018, **47**, 5266-5311.
4 W. Gong, Z. Chen, J. Dong, Y. Liu and Y. Cui, *Chem. Rev.*, 2022, **122**, 9078-9144.
5 M.M. Green and V. Jain, *Orig. Life Evol. Biosph.*, 2010, **40**, 111-118.
6 R.M. Flügel, *Chirality and Life – A Short Introduction to the Early Phases of Chemical Evolution*, Springer, Heidelberg, 2011.
7 D.P. Glavin, A.S. Burton, J.E. Elsila, J.C. Aponte and J.P. Dworkin, *Chem. Rev.*, 2020, **120**, 4660-4689.
8 L. Pasteur, *Ann. Chim. Phys., 3rd Ser.*, 1848, **24**, 442-459.
9 T. Shibata, H. Morioka,T. Hayase, K. Choji and K. Soai, *J. Am. Chem. Soc.*, 1996, **118**, 471-472.
10 C. Dressel, T. Reppe, M. Perhm, M. Brautzsch and C. Tschierske, *Nat. Chem.*, 2014, **6**, 971–977.
11 C. Dressel, F. Liu, M. Prehm, X. Zeng, G. Ungar and C. Tschierske, *Angew. Chem. Int. Ed.*, 2014, **53**, 13115–13120.
12 S. Kutsumizu, *Isr. J. Chem.*, 2012, **52**, 844-853.
13 Y. Nakazawa, Y. Yamamura, S. Kutsumizu and K. Saito, *J. Phys. Soc. Jpn.*, 2012, **81**, 094601.
14 Y. Cao, M. Alaasar, A. Nallapaneni, M. Salamończyk, P. Marinko, E. Gorecka, C. Tschierske, N. Liu, N. Vaupotič and C. Zhu, *Phys. Rev. Lett.*, 2020, **125**, 027801.
15 Y. Yamamura, Y. Nakazawa, S. Kutsumizu and K. Saito, *Phys. Chem. Chem. Phys.*, 2019, **21**, 23705-23712.
16 H. Schubert, J. Hauschild, D. Demus and S. Hoffmann, *Z. Chem.* 1978, **18**, 256-256.
17 H. Mori, S. Kutsumizu, T. Ito, M. Fukatami, K. Saito, K. Sakajiri and K. Moriya, *Chem. Lett.* 2006, **35**, 362-363.
18 S. Kutsumizu, H. Mori, M. Fukatami, S. Naito, K. Sakajiri and K. Saito, *Chem. Mater.*, 2008, **20**, 3675-3687.
19 G.W. Gray, B. Jones and F. Marson *J. Chem. Soc.* 1957, 393-401.
20 S. Kutsumizu, M. Yamada and S. Yano, *Liq. Cryst.*, 1994, **16**, 1109-1113.
21 S. Kutsumizu, T. Ichikawa, S. Nojima and S. Yano, *Chem. Commun.* 1999, 1181-1182.
22 S. Kutsumizu, K. Morita, T. Ichikawa, S. Yano, S. Nojima and T. Yamaguchi, *Liq. Cryst.* 2002, **29**, 1447-1458.
23 X. Zeng, L. Cseh, G.H. Mehl and G. Ungar, *J. Mater. Chem.*, 2008, **18**, 2953–2961.
24 K. Saito, Y. Yamamura, Y. Miwa and S. Kutsumizu, *Phys. Chem. Chem. Phys.*, 2016, **18**, 3280-3284.
25 X. Zeng and G. Ungar *J. Mater. Chem. C*, 2020, **8**, 5389-5398.
26 N. Vaupotič, M. Salamonczyk, J. Matraszek, M. Vogrin, D.

Pociecha and E. Gorecka, *Phys. Chem. Chem. Phys.*, 2020, **22**, 12814–12820.
27 Y. Sang, D. Yang, Z. Shen, P. Duan and M. Liu Mechanically Controlled and Consecutively Boosted Circularly Polarized Luminescence *J. Phys. Chem. C* 2020, **124**, 17274-17281.
28 Z.-G. Zheng, Y.-Q. Lu and Q. Li, *Adv. Mater.* 2020, **32**, 1905318.
29 T. Oka, *Acta Crystallogr. Sect. A*, 2022, **78**, 430–436.
30 T. Oka, *Acta Crystallogr. Sect. A*, 2023, **79**, 51-58.
31 N. Morimoto, K. Saito, Y. Morita, K. Nakasuji and M. Sorai *Liq. Cryst.* 1999, **26**, 219-228.
32 M. Sorai, and K. Saito, *Chem. Rec.*, 2003, **3**, 29-39.
33 K. Ozawa, Y. Yamamura, S. Yasuzuka, H. Mori, S. Kutsumizu and K. Saito, *J. Phys. Chem. B*, 2008, **112**, 12179-12181.
34 U. Shmueli, S.R. Hall and R.W. Grosse-Kunstleve, Symmetry in Reciprocal Space, in *International Tables for Crystallography, Volume B: Reciprocal Space, Second edition* (Ed. Shmueli, U.) Wiley, Weinheim, 2010, Chapter 1.4, pp. 114-174.
35 L. Öhrström and K. Larsson, *Molecule-Based Materials – The Structural Network Approach*, Elsevier, Amsterdam, 2005.
36 M.C. Holmes, *Curr. Opin. Colloid Interface Sci.*, 1998, **3**, 485-492.
37 L. Carlucci, G. Ciani, D.M. Proserpio and A. Sironi, *J. Am. Chem. Soc.*, 1995, **117**, 12861-12862.
38 L. Carlucci, G. Ciani, D.M. Proserpio and A. Sironi *Inorg. Chem.*, 1997, **36**, 1736-1737.
39 G. Friedel, *Ann. Phys.* 1922, **18**, 273-474.
40 L. Leibler, *Macromolecules*, 1980, **13**, 1602-1617.
41 T. Ohta and K. Kawasaki, *Macromolecules*, 1986, **19**, 2621-2632.
42 M.W. Matsen and F.S. Bates, *Macromolecules*, 1996, **29**, 1091-1098.
43 V.E. Podneks and I.W. Hamley, *JETP Lett.*, 1996, **64**, 617-624.
44 K. Saito, Y. Yamamura and S. Kutsumizu, *J. Phys. Soc. Jpn.*, 2008, **77**, 093601.
45 Y. Yamamura, R. Tsuchiya, S. Fujimura, M. Hishida and K. Saito, *J. Phys. Chem. B*, 2017, **121**, 1438-1447.
46 Y. Yamamura, M. Murakoshi, S. Iwagaki, N. Osiecka, H. Saitoh, M. Hishida, Z. Galewski, M. Massalska-Arodź and K. Saito, *Phys. Chem. Chem. Phys.*, 2017, **19**, 19434-19441.
47 Y. Yamamura, T. Murakoshi, M. Hishida and K. Saito, *Phys. Chem. Chem. Phys.*, 2017, **19**, 25518-25526.
48 K. Horiuchi, Y. Yamamura, R. Pełka, M. Sumita, S. Yasuzuka, M. Massalska-Arodz and K. Saito, *J. Phys. Chem. B*, 2010, **114**, 4870-4875.
49 Y. Yamamura, T. Adachi, T. Miyazawa, K. Horiuchi, M. Sumita, M. Massalska-Arodź, S. Urban and K. Saito, *J. Phys. Chem. B*, 2012, **116**, 9255-9260.
50 T. Adachi, H. Saitoh, Y. Yamamura, M. Hishida, M. Ueda, S. Ito and K. Saito, *Bull. Chem. Soc. Jpn.*, 2013, **86**, 1022-1027.
51 K. Saito, A. Sato and M. Sorai, *Liq. Cryst.*, 1998, **25**, 525-530.
52 S. Kutsumizu, K. Morita, S. Yano and S. Nojima, *Liq. Cryst.*, 2002, **29**, 1459-1468.
53 K. Saito and M. Sorai, *Chem. Phys. Lett.*, 2002, **366**, 56-61.
54 G.E. Schröder, S.J. Ramsden, A.G. Christy and S.T. Hyde, *Eur. Phys. J. B*, 2003, **35**, 551-564.
55 S. Hyde, S. Andersson, K. Larsson, Z. Blum, T. Landh, S. Lidin and B.W. Ninham, *The Language of Shape*, Elsevier, Amsterdam, 1997.
56 C. Dressel, T. Reppe, S. Poppe, M. Prehm, H. Lu, X. Zeng, G. Ungar and C. Tschierske, *Adv. Funct. Mater.*, 2020, **30**, 2004353.
57 T. Reppe, C. Dressel, S. Poppe and C. Tschierske, *Chem. Commun.*, 2020, **56**, 711-714.
58 T. Reppe, S. Poppe, X. Cai, Y. Cao, F. Liu and C. Tschierske, *Chem. Sci.*, 2020, **11**, 5902-5908.
59 O. Kwon, X. Cai, A. Saeed, F. Liu, S. Poppe and C. Tschierske, *Chem. Commun.*, 2021, **57**, 6491-6494.
60 M. Alaasar, X. Cai, F. Kraus, M. Giese, F. Liu and C. Tschierske, *J. Mol. Liq.*, 2022, **351**, 118597.